

# Trabajo de Fin de Master (TFM): Effect of the Electrostatic Environment in Majorana Nanowires

by

Samuel Díaz Escribano  
[samuel.diaze@estudiante.uam.es](mailto:samuel.diaze@estudiante.uam.es)

Master thesis advisors:

**Alfredo Levy Yeyati**  
*Dpto. Física Teórica de la Materia Condensada (UAM)*  
[a.l.yeyati@uam.es](mailto:a.l.yeyati@uam.es)

**Elsa Prada**  
*Dpto. Física de la Materia Condensada (UAM)*  
[elsa.prada@uam.es](mailto:elsa.prada@uam.es)

Universidad Autónoma de Madrid (UAM)

June 11, 2017

# TFM: Effect of the Electrostatic Environment in Majorana Nanowires

Samuel Díaz Escribano

Majoranas modes are exotic quasi-particles which have become a hot topic in condensed matter physics over the last few years. They emerge in non-trivial topological phases as non-local zero energy states at the edges of some specific materials, like quasi-one dimensional Rashba nanowires. The non-local nature of their wave function together with their non-Abelian statistics under exchange make them promising fault-tolerant qubits for quantum computation. However, spectroscopic measurements in real experiments exhibit some features that cannot be explained by simple theoretical models, such zero-energy pinning of the lowest lying modes or quantum dot like behavior. In this work we show that these features can be explained by taking into account the interaction of electrons in the nanowire with the bound charges that arise in the electrostatic environment. They make Majorana states more stable under magnetic and electrostatic perturbations, and they may also lead to the formation of quantum dots at the edges of the nanowires, which can be used as powerful spectroscopic tools to quantify the degree of Majorana non-locality.

## I. INTRODUCTION

In 1930 Paul Dirac<sup>[1]</sup> showed through the Dirac equation that there are four solutions for half-integer spin fermions: two solutions with the same energy (one for each spin), and another two solutions with the opposite charge and (negative) energy, called antiparticles. However, ten years later, Majorana<sup>[2]</sup> questioned the need to introduce a distinct antiparticle for each particle. He suggested the existence of a new kind of particles which constitute their own antiparticle, and therefore, they have to exist with zero energy and no charge. For the moment, Majorana's particles have not been discovered as elementary particles in nature<sup>[3]</sup>.

Despite this fact, solid state physicists have worked to find these particles as quasi-particles excitations in materials<sup>[4, 5]</sup>. The most promising devices where they could be found are Majorana nanowires<sup>[6–10]</sup>: one-dimensional (1D) materials in which the so-called topological superconductivity (TS) is induced. It is a mixture between a s-wave superconductor (SC) and some helical half-metal, which is a metal where each propagation direction has a single-degenerate carrier with opposite spin. A helical half-metal regime can be created by applying a large enough magnetic field to a semiconductor nanowire with a large spin-orbit coupling (Rashba effect). Furthermore, it has been recently shown that superconductivity can be induced by proximity effect into these structures<sup>[11, 12]</sup>. Hence, as theory predicts, the system could enter the TS phase by an appropriate tuning of the parameters like chemical potential and Zeeman field. Then, two majoranas quasi-particles appear at the nanowire edges at zero energy with a non-trivial topology<sup>[13]</sup>. This nanowire state is called Majorana nanowire.

Their zero-energy, non-local character of their wave function and their non-trivial topology make them a very suitable qubit for quantum computation<sup>[14, 15]</sup>: Majoranas can be combined in order to create a non-local coherent quantum state useful as a qubit for quantum computation; and because of their non-trivial topology

character they are topologically protected from decoherence by the environment.

Despite the efforts during the last years to develop a theory which explains the behavior of the Majorana nanowires, some discrepancies between theory and experiments are still present. The aim of our work is to explain some of these observed differences, such as zero energy anomalies. In order to do that, we are going to consider the interaction between the wire and the electrostatic environment<sup>[16, 17]</sup>. It has been recently shown that bound charges in the surrounding medium help retaining the zero energy characteristics of Majoranas under small magnetic and electrostatic perturbations<sup>[16]</sup>. Understanding it may help to exploit this feature, which can be a very powerful tool for quantum computation.

In the next sub-sections of the introduction, we present the standard theory for these 1D Majorana nanowires (Sect. I A) and the state of the art of the experimental status (Sect. I B), showing the discrepancies with the previous theory. In Sect. II we propose a physical mechanism that should take place in realistic experiments and that accounts for the experimental findings at odds with previous theory. Sect. II A and Sect. II B are devoted to understand some features that our results exhibit: pinning (Sec. II A), and unexpected energy levels behavior (Sect. II B). Finally the conclusions of our work are presented in Sect. III. Additionally, Appendix A explains the numerical methods used for our simulations and Appendix B obtains the electrostatic interaction between the environment and the nanowire.

### A. Standard Theory of Majorana Nanowire

The main ingredient to build these kinds of quasi-particles is superconductivity, which involves superpositions of electrons and holes, and violates charge conservation. Excitations of a conventional s-wave SC (described by the BCS theory<sup>[18]</sup>), take the form  $\gamma = uc_{\uparrow} + vc_{\downarrow}^{\dagger}$ , where  $u$  and  $v$  are the electron and hole components, and  $c^{\dagger}, c$  are the electron creation and annihilation operators.

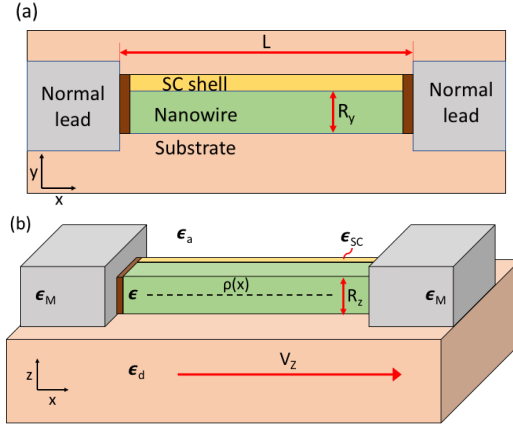


Figure 1. Top view (a) and partial side view (b) of the system considered in this work: a semiconductor nanowire with dielectric permittivity  $\epsilon$ , length  $L$ , and section  $R_y \times R_z$ , is placed over a substrate ( $\epsilon_d$ ), and contacted between two normal metal leads ( $\epsilon_M \rightarrow \infty$ ). One facet is covered by a SC shell ( $\epsilon_{SC}$ ), and it is surrounded by air otherwise. A magnetic field is applied along the  $x$ -axis. We model the nanowire charge density  $\rho(x)$  as a 1D charge density at its center along the  $x$ -axis. Potential barrier gates (brown) are used to measure the differential conductance.

We note that even if  $u = v^*$ , a  $\gamma$  excitation is different from  $\gamma^\dagger = v^* c_\downarrow + u^* c_\uparrow^\dagger = u c_\downarrow + v c_\uparrow^\dagger$  due to their spin. Hence, the aim is to find or create a SC which involves superpositions of electrons and holes with the same spin, so that excitations take the form:

$$\gamma = u c_\sigma^\dagger + v c_\sigma. \quad (1)$$

These operators satisfy  $\gamma^\dagger = \gamma$ , and thereby  $\gamma^\dagger \gamma = \gamma^2 = 1$  and  $\{\gamma_i, \gamma_j\} = 2\delta_{ij}$ . As a result of this last condition, Majoranas in condensed matter physics could not be conventional fermions (they do not obey Fermi-Dirac statistic [24]). This is why they are generally called Majorana zero modes (MZM) in solid state physics, instead of Majorana fermions.

In order to achieve Eq.(1) one method is mainly used for one-dimensional (1D) materials: inducing superconductivity and applying a magnetic field to a semiconductor with a large spin-orbit coupling (Rashba effect). S-wave SC can be induced to a semiconductor with a smaller pairing amplitude [11, 12] by proximity effect. P-wave component can also arise if the electrons of the semiconductor feel Rashba interaction, since it couples the electron spin and momentum [19]. If a (large enough) magnetic field is also applied, then the Zeeman splitting can fully spin-polarize the system, reaching a topological phase with a dominant p-wave superconductivity where MZM can emerge [4].

The most essential aspects of this system can be described using the following Hamiltonian written in Nambu representation:

$$\hat{H}_0 = [(\hbar^2 k_x^2 / 2m - \mu) \sigma_0 + \alpha \sigma_y k_x + V_Z \sigma_x] \tau_z + \Delta \sigma_y \tau_y,$$

where  $k$  is the electron momentum and  $m$  its effective mass,  $\mu$  is the chemical potential,  $\alpha$  the spin-orbit coupling amplitude,  $V_Z$  the Zeeman splitting,  $\Delta$  is the induced SC pairing amplitude [27], and  $\{\sigma_x, \sigma_y, \sigma_z\}$  the Pauli matrices in spin space, and  $\{\tau_x, \tau_y, \tau_z\}$  the Pauli matrices in electron-hole Nambu space. Matrices  $\sigma_0$  and  $\tau_0$  are their corresponding identities. A scheme of the system, as well as the chosen axis, are shown in Fig.(1).

The bulk dispersion relation (for an infinitely long nanowire) of this model is given by:

$$E_\pm^2 = \left( \frac{\hbar^2 k^2}{2m} - \mu \right)^2 + (\alpha k)^2 + V_z^2 + \Delta^2 \pm \pm 2 \sqrt{(\Delta V_z)^2 + ((\alpha k)^2 + V_z^2) \left( \frac{\hbar^2 k^2}{2m} - \mu \right)^2}. \quad (2)$$

Fig.(2a) shows the positive energies when some parameters are zero. When only the spin-orbit coupling plays a role ( $V_Z = 0$  and  $\Delta = 0$ ), the parabolic dispersion relation for a free electron is splitted into two (blue and red) parabolas. Each parabola has a different spin orientation since it depends on its momentum. If Zeeman splitting is also considered ( $\Delta = 0$ ), the two parabolas get splitted in energies (black curves): the one whose spin is aligned with the magnetic field, decreases its energy. Now, the chemical potential (dot line) can be fixed between the two curves, in order to reach an effective spinless phase. Finally, SC (gray line) pair electrons (and holes) with same spin. Nevertheless, owing to the competition between the Rashba and the Zeeman effect, the system will be just partially polarized in the remaining lower band.

Fig.(2b-d) shows Eq.(2) for different magnetic fields. As it is increased, the central gap closes at:

$$E_\pm = 0 \rightarrow V_Z^c \equiv \sqrt{\Delta^2 + \mu^2}. \quad (3)$$

At this point the system is spin-polarized, reaching a different topological phase. The change in the system topology is explained in Ref.[4]: a topological invariant associated to the energy bands can be defined. This parameter does not change under smooth perturbations, except if the topology changes. The topology of the system changes from a trivial state to a  $Z_2$  topological order (class D topological insulator) above  $V_Z^c$ . This non-trivial topology provides anyon character to the MZM [14]. Meanwhile, two midgaps keeps almost at the same energy, placed at (for  $\mu = 0$ ):

$$\left. \frac{\partial E_\pm^2}{\partial k} \right|_{k_F} = 0 \rightarrow k_F = \sqrt{2k_{SO}^2 + \sqrt{4k_{SO}^4 + k_Z^2}}, \quad (4)$$

where  $k_{SO} = m\alpha/\hbar^2$  and  $k_Z = \sqrt{2V_Z m}/\hbar$ . Fig.(2b-d) also shows that the larger the magnetic field is, the larger the difference between the energies  $E(k=0) \equiv \Delta_\pm \simeq \Delta \pm (V_z + \mu)$  are, so the bigger is the energy range where the chemical potential could be fixed in order to reach an effective spinless phase. However, the magnetic field has

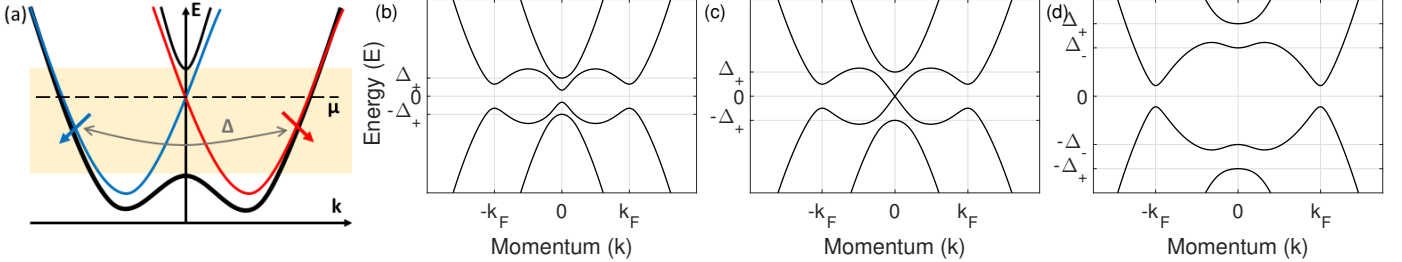


Figure 2. (a) Bulk dispersion relation of an infinite Rashba nanowire in the absence (blue and red curves) and in the presence (black curves) of a magnetic field. When the chemical potential  $\mu$  (dotted line) lies within the colored area, an effective spinless phase for the nanowire is reached. Superconductivity (gray line) can pair electrons with same spin then. Arrows indicate the electron spin direction, which follows the magnetic field except for the spin canting given by the spin-orbit interaction term. (b-d) Nambu representation of the dispersion relation of the same wire in the presence of an induced superconducting pairing  $\Delta$ , for different magnetic fields: (b) before the topological phase transition  $V_Z = 0.5V_Z^c$ ; (c) at the gap closing  $V_Z = V_Z^c$ ; (d) after the topological transition  $V_Z = 1.5V_Z^c$ , where  $V_Z^c \equiv \sqrt{\Delta^2 + \mu^2}$ . We have defined  $\Delta_{\pm} \equiv \Delta \pm (V_z + \mu)$ .

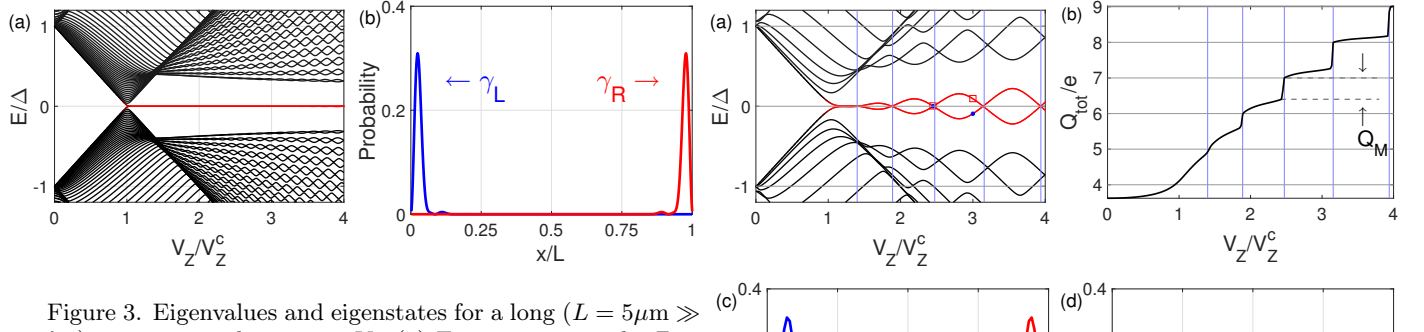


Figure 3. Eigenvalues and eigenstates for a long ( $L = 5\mu\text{m} \gg \lambda_F$ ) nanowire with  $\mu = 0\text{meV}$ . (a) Energies versus the Zeeman splitting. The two red modes are the MZM; (b) wave functions of the two lowest energy modes at  $V_Z = V_Z^c$ . For a long nanowire, the Majorana wave functions are similar for any  $V_Z > V_Z^c$ , whereas the wave function of the higher energy levels (black) varies strongly. We represent in blue the left Majorana  $\gamma_{\text{Left}}$ , and in the red the right one  $\gamma_{\text{Right}}$ .

to be smaller than the critical magnetic field of the SC. Otherwise, superconductivity would be destroyed. Because Zeeman splitting takes the form  $V_Z = \mu_B g B / 2$ , where  $\mu_B$  is the Bohr's magneton,  $g$  the Landé  $g$ -factor, and  $B$  the magnetic field; then it is not necessary to apply a high magnetic field if  $g$  is large enough, as it happens in some semiconductor materials[20].

We want to study now realistic finite nanowires. In order to do that, the nanowire has been discretized using a tight-binding model (see Appendix A for more detail). Fig.(3a) shows the energies versus the Zeeman splitting for a very long nanowire (when  $L \gg \lambda_F = 2\pi/k_F$ ), which in practice can be still considered as infinite. At zero magnetic field, there is a gap between  $(-\Delta, \Delta)$  due to the induced superconductivity. All energy levels are spin-degenerate. When the magnetic field is increased, the energy levels split due to the Zeeman effect: those whose spin is aligned with the magnetic field go down in energy. At  $V_Z = V_Z^c$  the gap closes at zero energy, keeping two states (red) at this zero energy. Because these zero modes

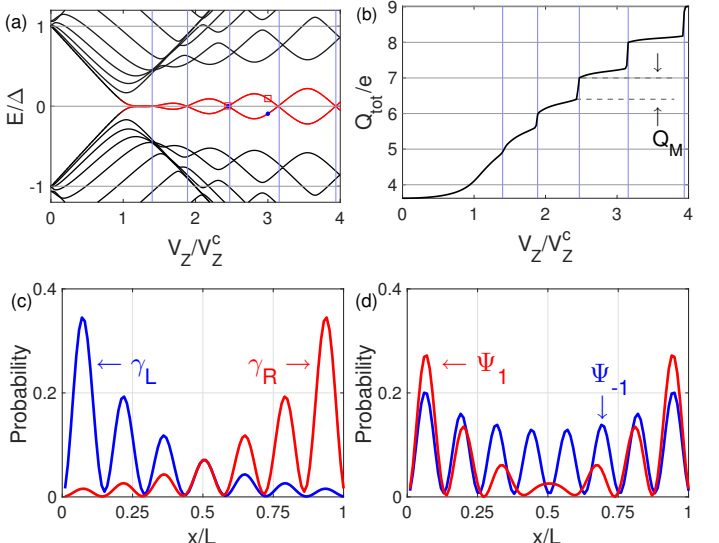


Figure 4. Energy spectrum (a) and total charge (b) versus the Zeeman splitting for a short ( $L = 1\mu\text{m} \sim \lambda_F$ ) nanowire with  $\mu = 0\text{meV}$ . Vertical blue lines indicate the position of the parity crossings. Majorana wave function at the parity-crossing (c) and at  $V_Z = 3V_Z^c$  (d), both marked by dots and squares in (a). Each dot/square color in (a) corresponds to each eigenstate color in (c) and (d).

are topologically protected, no energy levels can cross them. Hence, a gap between the remaining bands and these zero energy levels is open for  $V_Z > V_Z^c$ . Since a wire in a topological phase naturally forms a boundary with a trivial state (the vacuum), edge states has to emerge at the ends of the wire at this (zero) energy (see Fig.(3b))<sup>[8]</sup>. These two states left  $\gamma_L$  and right  $\gamma_R$  are just the MZM.

Nevertheless, this is not completely true for a short nanowire (when  $L \sim \lambda_F$ ). Fig.(4a) shows the energies versus the Zeeman splitting for a  $L = 1\mu\text{m}$  nanowire. There are no modes staying at zero energy, but there are two (red) energy levels oscillating instead. In each

crossing (called parity crossing), the total charge of the wire increases abruptly by an amount  $Q_M$  (total charge is plotted in Fig.(4b)). The lowest-energy eigenstates in a parity crossing are shown in Fig.(4c). Eigenstates exhibit oscillations with periodicity  $\lambda_F/2$  from each end of the nanowire due to  $V_Z$ ,  $\mu$  and  $\alpha$ . They are not fully localized at the edges of the wire, but they decay exponentially into the nanowire center with a decaying length [13] given by  $h\nu_F/\Delta = h\sqrt{2V_Z}/\Delta\sqrt{m}$ . Both eigenstates are orthogonal since  $\lambda_F/2$  is an integer multiple of the length. Outside a parity crossing (Fig.(4d)) this is not true: because  $\lambda_F/2$  is not an integer multiple of the length, they are not orthogonal. MZM are no longer eigenstates but they hybridize into two Nambu eigenstates with different parity  $\Psi_1 = \Psi_M = (\gamma_L + i\gamma_R)/2$  and  $\Psi_{-1} = \Psi_M^\dagger = (\gamma_L - i\gamma_R)/2$  whose energies oscillates around zero depending on their degree of overlap. In each parity crossing, the equilibrium-occupation of the  $\Psi_M$  quasiparticle changes abruptly (as well as its parity), and the total charge of the wire increases in a non-quantized way:

$$\begin{aligned} Q_M &= |Q_1 - Q_{-1}| = \\ &= \frac{e}{4} \int_0^L dx \left[ |u_L^*(x) + iu_R^*(x)|^2 - |u_L^*(x) - iu_R^*(x)|^2 \right] = \\ &= e \int_0^L dx |u_L(x) u_R(x)|. \quad (5) \end{aligned}$$

Thus, the charge of this Majorana state  $\Psi_M$  is non-zero despite it is a superposition of two neutral MZM owing to the spatial overlap between both.

## B. Experimental status

It has been theoretically shown that Majoranas appear in 1D systems at zero energy on each side of the wire, at magnetic fields larger than  $V_Z^c$ . It has been also shown how energy levels behave when the magnetic field is changed. Both elements can be used to detect MZM experimentally. However, measuring something at zero energy is often difficult. For this reason, most of the experimental researches use the same technique: tunneling spectroscopy. This tool measures the differential conductance  $dG = dI/dV$  between the ends of the wire by measuring the current  $I$  at a certain applied voltage  $V$ . This conductance is roughly proportional to the density of states of the system, which directly measures the number of accessible states at energy  $V$ . Hence, experiments should show a zero-bias peak (ZBP) on each side of the wire for the differential conductance [28].

During the last five years, experiments using this method have been performed [6-10]. Experimental results of Ref.[7] are shown in Fig.(5a). The nanowire (green) is made of InAs, a semiconductor which is known to have strong spin-orbit interaction and a large g factor. It is growth over a  $\text{SiO}_2$  substrate. A thin SC layer of Aluminum (blue) only cover the third part of the nanowire,

avoiding complete screening of the underlying gates (yellow), which are used to change the applied voltage  $V_G$  (chemical potential). Two Ti/Au normal leads (yellow) attached on each side of the nanowire are used for measuring the differential conductance.

Fig.(5b) shows the differential conductance versus voltage at 50mK taken at different magnetic fields. There is a  $\sim 0.2\text{meV}$  SC pairing, as it can be seen at zero magnetic field through the gap. At a certain magnetic field ( $\sim 200\text{mT}$ ), one peak emerges at zero energy, which oscillates around this energy for larger magnetic fields. This ZBP is arguably the MZM, but there are many other low-energy phenomena that could lead to a ZBP. For this reason, the researchers have considered various options which could explain this ZBP, as the Kondo effect or Andreev Bound States (ABS). However, ZBP due to the Kondo effect or ABS should split and move to finite energy when the magnetic field is changed. Hence, they conclude that this ZBP is the MZM.

However the behavior of the energy levels seems not to be totally in agreement with the theory: the first ZBP at 200mT pins at zero energy for almost 100mT, instead of being just a crossing point. Another experiments exhibit also this behavior. This is the case of Ref.[8] which their experimental set-up is shown in Fig.(5c): a nanowire made of InSb, also known for its strong spin-orbit interaction and a large g factor, is coverage by a SC shell of NbTiN (yellow), which has a large SC critical magnetic field. One Ag normal lead (magenta) together with a barrier gate (orange) is used for measuring the differential conductance.

Fig.(5d) shows the corresponding differential conductance versus voltage at 50mK taken at different magnetic fields. The induced gap is close to  $0.4\text{meV}$ , as it can be seen at zero magnetic field. At a certain Zeeman splitting ( $\sim 0.4\text{meV}$ ), one peak emerges at zero energy. But, in this experiment, this peak seems to be pinned at zero energy for, at least, 300mT: at  $0.75\text{T}$  the ZBP seems to be wider and blurrier. This could be one energy oscillation, but of course, it is smaller than those predicted by the theory. It also shows pinned regions that theory is not able to explain.

The aim of our work is to explain the above mentioned discrepancy between theory and experiments following the ideas of Ref.[16]. We have seen that each parity-crossing introduces a charge  $Q_M$  into the system. Then, if the dielectric environment is repulsive ( $\epsilon_{\text{environment}} < \epsilon_{\text{wire}}$ ), bound charges of the same sign arise in the environment (SC shell, leads, substrate and/or air or vacuum). It creates a repulsive “self”-interaction between these bound charges and the real one, whose entrance into the nanowire is then suppressed, leading to MZM pinned regions.

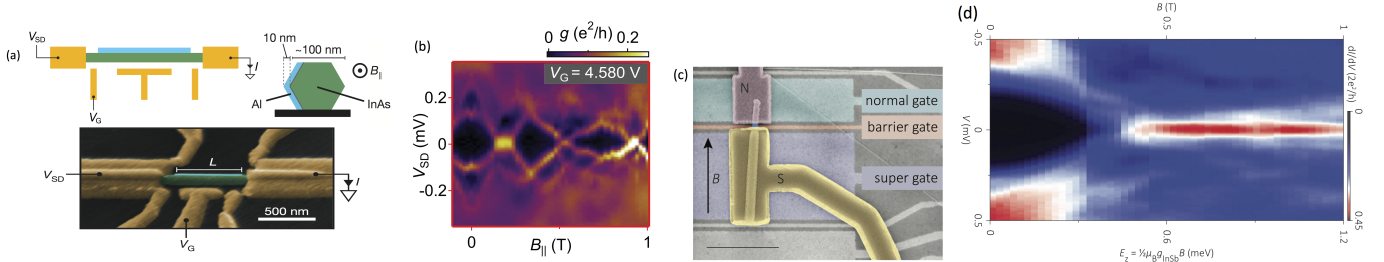


Figure 5. (a-b) Experiment reported in Ref. [7]: (a) Experimental set up: an hexagonal InAs nanowire (green) growth over a  $\text{SiO}_2$  substrate (black), with a SC Al shell (blue), and Ti/Au gates (yellow). The differential conductance can be measured through the current  $I$  at a certain source-drain voltage  $V_{SD}$ . The  $V_G$  voltage fixes the chemical potential; (b) Experimental result: Conductance  $G = I/V_{SD}$  versus magnetic field and  $V_{SD}$  gate. (c-d) Experiment reported in Ref. [8]: (c) Experimental set up: an hexagonal InSb nanowire growth over a  $\text{SiO}_2$  substrate (gray), with a SC NbTiN (yellow), and one Ag normal lead (magenta), which together with a barrier gate (orange) is used for measuring the differential conductance; (d) Experimental result: differential conductance versus magnetic field (upper axis) or Zeeman splitting (bottom axis) and voltage bias.

## II. RESULTS

We treat interactions between the electrostatic environment at a self-consistent Poisson mean field level. The interacting hamiltonian is given by  $\hat{H} = \hat{H}_0 + e\phi_b(x)\sigma_0\tau_z$ , where  $e$  is the electron charge, and  $\phi_b(x)$  is the self-consistent electrostatic potential created by bound charges,

$$\phi_b(x) = \int dx' V_b(x, x') \langle \hat{\rho}(x') \rangle. \quad (6)$$

Here,  $\langle \hat{\rho}(x') \rangle$  is the quantum and thermal average of the nanowire charge density, and  $V_b(x, x')$  encodes the geometry information of the electrostatic interaction between a charge placed at  $x$ , and the bound charges created at the dielectric medium at  $x'$  (so  $V_b$  is the kernel of the interaction). Following the experimental set-up of Ref. [7], the electrostatic medium has been described as shown in Fig. (1): the nanowire is described by a rectangular wire with dielectric permittivity  $\epsilon$ , length  $L$  and width  $R$ . We model the charge density  $\rho(\vec{r})$  of the nanowire as a charge density line at its center. The nanowire has six interfaces (one at each facet): at bottom a  $\text{SiO}_2$  dielectric substrate with dielectric permittivity  $\epsilon_d = 3.9$ ; on the upper facet and on one side there is vacuum or some gas (like Helium) with dielectric permittivity  $\epsilon \simeq 1$ ; on the other side is placed the SC shell; and at both edges of the wire a normal metal emulates the leads. The “dielectric” permittivity for the normal leads can be taken as positive and infinite  $\epsilon_M \rightarrow \infty$ , because we are assuming a quasi-static interaction and normal leads have metal bulk properties. However, this is not true for the SC shell: because it is an ultra-thin film of  $\sim 6\text{nm}$  of thickness, the “dielectric” permittivity is finite [21]. It has been shown that it could be of the order of  $\epsilon_{SC} \simeq 100$ , which is still a large number. Taking into account this electrostatic environment,  $V_b$  is obtained in Appendix B using the image charge method. Then the potential  $\phi_b(x)$  can be solved self-consistently using numerical methods (see Appendix A for more details).

We want to study the interaction between the nanowire and the electrostatic environment. We first consider that the nanowire is isolated from the leads (due to the tunnel barriers), so that we first ignore the interaction with the left-right leads  $H_A$  in Sec. II A as a first approximation to the problem. Then, the full-model  $H_B$  (including the interaction with the leads) is going to be studied in Sec. II B.

### A. First approach to the electrostatic environment interaction

The wire energy levels versus Zeeman splitting excluding the interaction with the leads for  $\mu = 0.5\text{meV}$  are shown in Fig. (6b). It can be compared with the non-interacting one in Fig. (6a). Pinned regions (red) of  $\sim 0.5\text{meV}$  width can be seen at  $\{1, 1.5, 2.5, 3.5\} \text{ meV}$ . It is known that each parity crossing injects a charge  $Q_M$  of the same sign into the system. This charge has to create bound charges into the dielectric medium, making, as a result, a rapid increase of the repulsive electrostatic potential felt by the electrons. The potential is shown in Fig. (6c), where red lines correspond to the pinned regions. The potential is mainly repulsive since it is positive for the most part of the nanowire. The spacing between the red lines is larger than between the gray ones despite the jump in the magnetic field is the same. Hence, the electrostatic potential is increasing faster in the (red) pinned regions. Fig. (6d) shows the total charge for this interacting system (in solid lines), which can be compared with the non-interacting one (dashed lines). While the non-interacting one exhibits charge jumps (as it has been discussed in Sec. I A), the charge in the interacting system turns into extended (red) regions where the charge come into the nanowire progressively, as the magnetic field increases. This means that bound charges are conspiring to suppress the charging, pinning the energy of the MZM at zero energy, and freezing their wavefunctions. Deviations from exactly zero energy pinning may arise for finite

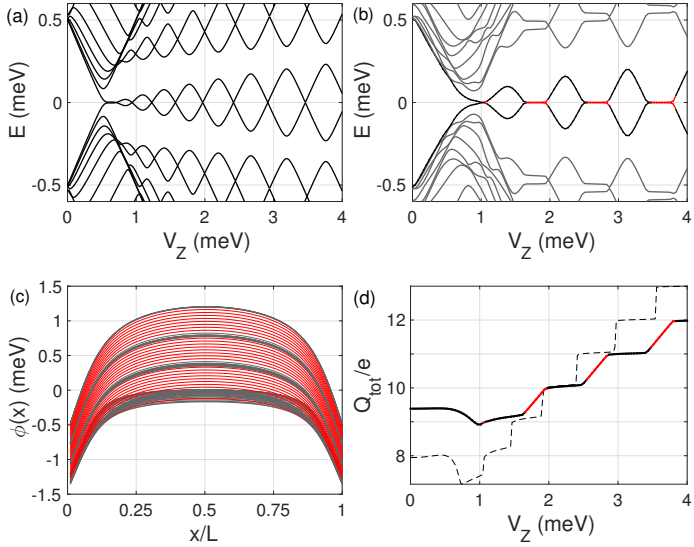


Figure 6. Energy levels versus the Zeeman splitting for the non-interacting  $H_0$  (a) and interacting  $H_A$  (without the leads) (b) nanowire. (c) Self-consistent solution of the electrostatic potential as a function of the wire position  $x$ . (d) Total charge of the nanowire versus the Zeeman splitting for the non-interacting  $H_0$  (dashed curve) and interacting  $H_A$  (solid curve) nanowire. In all previous panels  $R_y = R_z = 50\text{nm}$ ,  $L = 1\mu\text{m}$  and  $\mu = 0.5\text{meV}$ . Red lines mark pinned regions.

temperature such as  $T = 10\text{mK}$  taken in our simulations.

Although we have taken  $\mu = 0.5\text{meV}$  for our simulations, pinning is general for all chemical potentials, as it can be seen in Fig.(7b). There the pinned regions across the  $V_Z - \mu$  space are shown (in red). They can be compared with the parity-crossings for the non-interacting system in Fig.(7a). We note that parity crossings evolve to finite width pinning regions through all the topological  $V_Z - \mu$  space. Pinning regions are bigger for lower chemical potentials and for higher magnetic fields, since the repulsive interaction is larger too. It can be seen that the beginning of the topological phase is different between the interacting system and the non-interacting one (black dot lines). This is because the electrostatic potential is renormalizing the chemical potential[17], so it has to be also included in the critical magnetic field:

$$V_Z^c(x, V_Z) = \sqrt{(\mu - \phi_b(x))^2 + \Delta^2}. \quad (7)$$

We note that this equation can not be solved analytically because  $V_Z$  depends on  $\phi_b(x)$ . The behavior of the parity crossings versus  $V_Z - \mu$  is also different between both systems (interacting and non-interacting) due to the renormalization of the chemical potential as well.

However, pinning is not general for all kind of environments. Fig.(7c) shows also the incompressible regions but across the  $V_Z - \epsilon_{SC}$  space ( $\mu - \epsilon_{SC}$  space exhibit a similar behavior). Different values for  $\epsilon_{SC}$  means different widths for the SC shell, or different SC mediums. Around  $\epsilon_{SC} \sim 250$ , pinning width turns into points (the

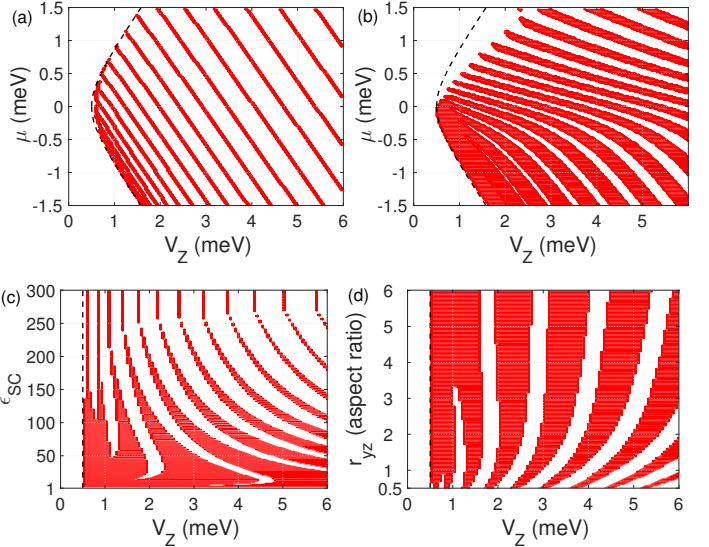


Figure 7. Nanowire phase diagram versus  $\mu$  and  $V_Z$  with zero energy solutions marked in red (for  $L = 1\mu\text{m}$  and  $R_y = R_z = 50\text{nm}$ ) for the non-interacting  $H_0$  (a) and interacting  $H$  (b) cases. Parity crossing lines in (a) evolve to extended regions in (b). Pinned regions (red) with  $\mu = 0$  versus  $V_Z$  and (c) versus the dielectric permittivity of the SC shell  $\epsilon_{SC}$ , and (d) versus the aspect ratio  $r_{yz} = R_y/R_z$  of the nanowire, where  $R_z = 50\text{nm}$  is fixed. Dashed black lines indicate the beginning of the non-interacting topological transition.

parity crossings) because the electrostatic environment turns into an attractive one. This means bound charges of the opposite sign arise in the dielectric medium at these large permittivities, so charging the nanowire is now more favored (instead of being suppressed). The width of the nanowire also plays a role in the pinning. Fig.(7d) shows the incompressible regions along the  $V_Z - r_{yz}$  space, where  $r_{yz}$  is the aspect ratio of the nanowire section. When the distance between the SC shell and the opposite side is large (large  $r_{yz}$ ), the pinning is bigger. This is because the SC shell is farther from the center of the nanowire, so the attractive interaction is weaker.

## B. Full model for the electrostatic environment interaction

The results including now the interaction with the leads  $H_B$  for  $\mu = 0.5\text{meV}$  are shown in Fig.(8a). While (red) pinned regions for the MZM energy levels are still present (although they are smaller), another feature emerges: four (blue) energy levels detach from the quasi-continuum above the mid-gap, approach zero energy at 2meV and anti-cross with the MZM. An extra zero-energy crossing is induced by these energy levels at 2meV. The total charge of the full model system (shown in Fig.(8b)) also exhibits another unexpected behavior: while the increasing jumps seen in the previous section (Fig.(6d)) are still present at each parity-crossings, it can be seen that

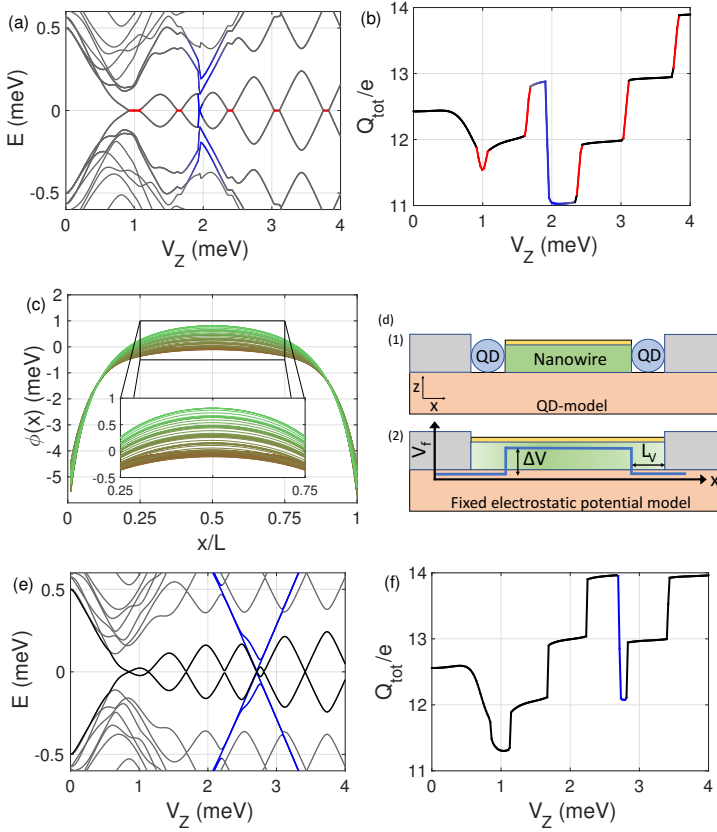


Figure 8. (a-c) Nanowire in the regime described by the full-model interacting Hamiltonian  $H_B$  between the nanowire and the electrostatic environment with  $L = 1\mu\text{m}$ ,  $R_y = R_z = 50\text{nm}$  and  $\mu = 0.5\text{meV}$ . Energy spectrum (a) and total charge (b) versus Zeeman splitting. Electrostatic potential (c) versus nanowire position  $x$ . Color grading indicates the magnitude of the magnetic field, from  $V_Z = 0\text{meV}$  in brown to  $V_Z = 4\text{meV}$  in green. (d1) Sketch of the QD-nanowire model and (d2) sketch of the fixed electrostatic potential model. Energy spectrum (e) and total charge (f) versus Zeeman splitting for the fixed electrostatic potential model with  $\Delta V = -3\text{meV}$  and  $L_V = 140\text{nm}$ . Blue energy levels are levels approaching to zero energy after the topological transition (QDEL).

charge is expelled at this point (2meV). The electrostatic potential (see Fig.(8c)) is now repulsive at the middle of the nanowire but it is attractive at the edges, with a energy difference of 5meV (ten times bigger than other energy scales, such as  $\mu$  and  $\Delta$ ).

Because  $\phi_b(x)$  depends strongly on position  $x$ , then the topological transition does too, as Eq.(7) shows. This implies that the nanowire is entering the topological phase by regions: first the center of the nanowire enters the topological phase at  $V_Z \simeq 0.75\text{meV}$ , and then, the rest of the nanowire does progressively as the magnetic field increases. Because the (blue) unexpected energy levels do not follow the typical energy levels behavior for a topological nanowire seen in Sect.IA they have to come from this outer nanowire region outside the topological phase. In such situation, Majoranas are just located

at the edges of the nanowire region that is inside the topological phase. When the nanowire region inside the topological phase is increased (as a result of a magnetic field increasing), Fig.(8b) shows that charge is being expelled from this outer region. One might think that the electron-electron interaction among the nanowire electrons (that we have neglected so far) could destroy the attractive interaction of this outer regions, making  $\phi_b(x)$  flatter. We have performed numerical simulations (not shown here) that prove that this interaction is not strong enough to destroy this feature.

The energy spectrum behavior of Fig.(8a) has been found in some experimental works[7 22], and has also emerged in the study of hetero-structures devices of Majorana nanowires coupled to quantum-dots (QD)[23, 24] (see Fig.(8d) for a sketch of the system). In these works, the authors conjecture that these energy levels approaching to zero energy are the QD energy levels hybridizing with the Majorana nanowire ones. For this reason, we say that these unexpected energy levels behavior follow a QD energy level like behavior (QDEL).

In order to understand the behavior of the QDELS which emerge in our system, we have developed a simplified model: because QDEL comes from the topological phase differences in the nanowire (due to the non-uniform electrostatic potential profile), a system with a fixed non-homogenous electrostatic (or chemical) potential should reproduce the results. This non-homogeneity has been taken as much similar as the electrostatic potential exhibits in Fig.(8c), trying to take it as much simple as possible too. Thus, we have studied the effect of a fixed electrostatic potential  $V_f$  with the shape of two finite wells at the edges of the nanowire (see Fig.(8d)):

$$V_f = \Delta V [1 - \Theta(x - L_V) + \Theta(x - L + L_V)], \quad (8)$$

where  $\Delta V$  is the depth of the potential well,  $L_V$  its width, and  $\Theta(x)$  the Heaviside function. These potential wells could be understood as QDs too. Fig.(8e) shows the energies of this system versus the Zeeman splitting. QDEL can be seen in blue lines approaching zero energy at almost 2.5meV. At this point, QDEL seems to pin the MZM to zero energy, breaking the energy oscillations. This is a general feature observed at these points where the QDEL goes close to zero energy. It has been shown in Sect.IA that the energy splitting of the MZM is given by the degree of overlap between the two Majoranas. Now these two quasi-particles are hybridized with the QD modes too, so the energy is given by the degree of overlap between these six states (one electron an one hole energy level for each QD, and the two MZM), and their charge is given by the degree of overlap between them too. Total charge of the nanowire is shown in Fig.(8f). When the QDEL goes near to zero energy, the charge is expelled, as the full-interacting model also exhibits in Fig.(8b).

At this point, some questions arise which should be answered in future works in order to have a deeper understanding of the problem: how do MZM wavefunctions

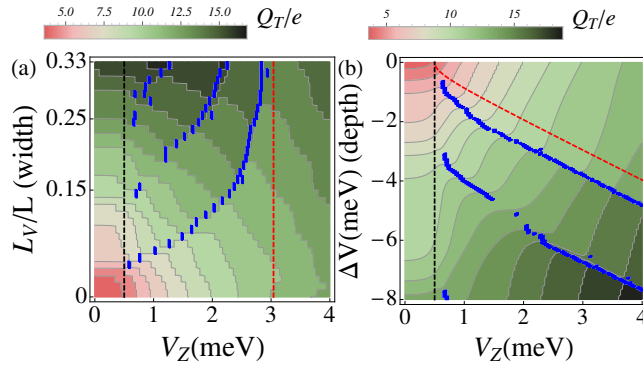


Figure 9. Total charge of the fixed electrostatic potential model (with  $\mu = 0\text{meV}$  and  $L = 1\mu\text{m}$ ) versus the Zeeman splitting and: (a) versus the width (with  $\Delta V = -3\text{meV}$ ), or (b) versus the depth of the potential wells (with  $L_V = 140\text{nm}$ ). Black dashed lines correspond to the topological transition of the nanowire center, red dashed lines correspond to the topological transition of the potential wells, and blue points mark the minimum of the QDBs (where charge is expelled).

behave at these points where QDEL approach zero energy? Why is charge expelled? If both states are hybridized, is the topological protection of MZM broken?

We are going to focus now just in the behavior of the QDEL (rather than in its effect over the MZM). The minimum of the QDEL (blue) and the total charge for the  $V_Z - \mu$  space is shown versus the width and the depth of the electrostatic potential wells in Fig.(9a) and Fig.(9b). Both could be tuned experimentally using a potential gate or different lead geometries. The stronger interaction, the deeper and wider are the potential wells. The topological transition for the nanowire center (fixed  $\mu = 0\text{meV}$ ) happens at the black dashed lines, and the red ones mark the transition for the nanowire region inside the potential wells, whose chemical potential is given by  $\Delta V$ . Outside the region limited by the dashed lines there is no QDELS approaching to zero energy (blue points). This is because the topology is equal for the entire nanowire: before the black line the full nanowire is in the topological trivial phase, and after the red one in the non-trivial phase. Hence, no charge can be expelled. Between these two transitions some QDELS emerge due to the non-homogenous topological phase of the nanowire. At these points, charge is expelled from these regions inside the potential wells. Their position in this space change because a change in the chemical potential  $\Delta V$  or a change in the potential well length  $L_V$ , changes the QD energy levels.

### III. CONCLUSIONS

It has been shown that Majoranas (in solid state physics context) can emerge as zero-energy modes (MZM) on 1D systems, such as Rashba nanowires with

induced superconductivity in the presence of an external magnetic field. These MZM are edge states appearing at the interface between the trivial topological phase of the vacuum and the non-trivial topological phase of the nanowire. Experiments showing zero energy anomalies compatible with MZM are more robust than theory predicts. This is manifested through zero energy pinning regions for magnetic field and/or chemical potential perturbations. It is also known that a finite energy splitting and charge of the MZM are due to the overlapping between both wave functions.

Motivated by this theory-experiment disagreement, we have studied the electrostatic environment effect on the Majorana nanowire. We have shown that bound charges in a repulsive dielectric medium prevent electrons from entering into the nanowire because of the interaction between the MZMs and their image charges in the environment. Hence, the overlapping between both MZMs is prevented for some magnetic range, pinning MZM at zero energy for this range. It has been also shown that quantum-dots (QD) are naturally built in at the edges of the nanowire, as a result of a non-homogenous electrostatic potential. This electrostatic potential is attractive at the nanowire edges due to the proximity of metal leads, while it is repulsive in the middle of the nanowire due to the remaining environment. This causes the nanowire to transition into the topological phase at the middle region first, and then, gradually at the edges. When the topology is trivial at the nanowire ends, the corresponding energy levels hybridize with the non-trivial topological energy states of the nanowire middle. It creates QD energy levels like (QDEL) which can interfere the MZM energy oscillations, as well as to expel charge outside the nanowire. However, the mechanism whereby it happens is not totally clear. We note that a deeper study of the eigenstates of a coupled QD-Majorana system is still required, in order to understand this phenomena.

Pinning and QDEL can be useful for quantum computation, since MZM can be used as qubits[14, 15]. Both features can be experimentally exploited using different nanowire geometries or materials. We have shown that pinning is a generic feature which can be increased if the electrostatic environment is repulsive. Hence, making thinner or smaller SC shells, screening electrostatic lead interaction, or choosing a nanowire with a larger dielectric permittivity, should produce larger pinned regions, and therefore, MZM should be more robust against magnetic and chemical potential perturbations. We also note that the permittivities used in our simulations are rough estimates, their actual values for the thin films and nanowires in actual experiments are unknown. QDs have been recently shown[23] to be a powerful spectroscopic tool in order to quantify the degree of Majorana non-locality. We have shown QDEL can be tuned using different geometries for the leads, which could change the strength and the range of the electrostatic lead interaction.

*Acknowledgments.*— I want to strongly thank Alfredo

Levy Yeyati and Elsa Prada for the time they have spent leading my TFM, as well as their support.

## Appendix A: Numerical Methods

In order to transform Hamiltonian  $H_0$  to real space, momentum operator has been transformed into real space using the identity  $k_x \rightarrow -i\hbar\partial/\partial_x$ . The nanowire has been taken as a 1D discretized lattice, which allows spatial partial derivates to be rewriting as  $\partial/\partial_x \rightarrow (c_{j+1}^\dagger c_j - c_{j-1}^\dagger c_j)/a$ , where  $c_j^\dagger, c_j$  are the creation and annihilation operators in the lattice position  $j$ , and  $a$  is the lattice spacing, always equal to 10nm in our simulations. Then, the real space hamiltonian is given by:

$$\hat{H}_0 = \frac{1}{2} \sum_j \left( \psi_j^\dagger \hat{h}_1 \psi_j + \psi_{j+1}^\dagger \hat{h}_2 \psi_j + \psi_{j-1}^\dagger \hat{h}_2 \psi_j \right), \quad (\text{A1})$$

where  $\psi_j^\dagger = (c_{j\uparrow}^\dagger, c_{j\downarrow}^\dagger, c_{j\uparrow}, c_{j\downarrow})$  is the on-site Nambu bi-spinor,  $\hat{h}_1 \equiv [(2t - \mu) \sigma_0 + V_Z \sigma_x] \tau_z + \Delta \sigma_y \tau_y$  and  $\hat{h}_2 \equiv -(t \sigma_0 + i \alpha_R \sigma_y) \tau_z$  are spin-Nambu space Hamiltonians,  $t \equiv \hbar^2/2ma^2$  is the hopping parameter, and the Rashba constant in real space is  $\alpha_R \equiv \alpha \hbar/2a$ . Rashba constant for semiconductor materials (like InAs) is thought [6, 8] to be between 20 – 50meV · nm, and it has been performed [12] induced SC gaps between  $\Delta = 0.5 - 0.2$ meV. For our simulations, it has been taken an effective mass of  $m = 0.015m_e$ , a Rashba constant of  $\alpha = 20$ meV · nm, and a SC gap of  $\Delta = 0.5$ meV. Most of the grown nanowires are  $L = 1\mu\text{m}$ , with an hexagonal section of  $R = 50$ nm width. We have assumed a rectangular section in our simulations for simplicity. Eigenvalues  $\epsilon_n$  and their corresponding eigenstates  $\Psi_n = (u^{(n)}, v^{(n)})$  for the hamiltonian of Eq. (A1) have been obtained using *Matlab*. Here  $u^{(n)}$  and  $v^{(n)}$  is the electron and hole component along the full nanowire of the  $\Psi_n$  Bogoliubov eigenstate. Thus, the total charge of the nanowire is given by:

$$\begin{aligned} Q_T &= \sum_n Q^{(n)} = \sum_n \langle \hat{\rho}_n \rangle = \sum_n e \langle \Psi_n^\dagger \Psi_n \rangle = \\ &= \sum_n e \int f(\epsilon_n) |u^{(n)}|^2 + f(-\epsilon_n) |v^{(n)}|^2, \end{aligned} \quad (\text{A2})$$

where  $\langle \dots \rangle$  means quantum and thermal average,  $\rho_n$  is the charge density of the  $n$ -th eigenstate, and  $f(E) = 1/(1 + e^{-E/k_B T})$  is the Fermi-Dirac distribution function, where  $k_B$  is the Boltzmann constant, and  $T$  the temperature taken as 10mK in our simulations.

Hamiltonians seen in the main text  $H_A$  and  $H_B$  can not be diagonalized analytically because they depend on their own eigenstates. For this reason, we found its eigenstates using a self-consistent numeric method (with an adaptive update coefficient), taking the probability density of the  $H_0$  hamiltonian for the first self-consistent iteration as

a test solutions, and then, taking the output probability densities for the next iterations. We considered that it converges when, at least, there was no change in the fourth decimal number for all the eigenvalues (energies). All constants and the potential in the nanowire middle  $\phi(V_Z = 0, x = L/2)$  have been neglected, because they just renormalize the chemical potential.

## Appendix B: Electron-environment interaction

The electrostatic interaction between the nanowire and the dielectric medium is given by the bound charges created at the surrounding medium shown in Fig. (1). In order to give more insight on the solution of this problem, we are going to solve first some simpler problems. We are going to solve them using the electrostatic image charge method [25].

*One infinite facet.*— The solution to this problem can be found in any university student's book of electromagnetism [25]: when just one charge  $q$  is placed in the nanowire at a distance  $R$  from the interface between the nanowire and a dielectric material with dielectric permittivity  $\epsilon_d$ , then the classical electrostatic potential due to the bound charges takes the form:

$$\phi_b(x) = \frac{1}{4\pi\epsilon\epsilon_0} \frac{\kappa_d q}{\sqrt{(2R)^2 + x^2}}, \quad (\text{B1})$$

where:

$$\kappa_\alpha \equiv \frac{\epsilon - \epsilon_\alpha}{\epsilon + \epsilon_\alpha}. \quad (\text{B2})$$

This bound charge is equivalent to a charge  $\kappa_d q$  place at the same distance  $R$  from the interface, but inside the dielectric. Because of that, it can be understood as an image charge seen by the original charge through the interface. Because  $\phi_b$  is linear with  $q$ , this result may be generalized to an arbitrary 1D density charge  $\rho(x)$ :

$$\phi_b(x) = \frac{1}{4\pi\epsilon\epsilon_0} \int \frac{\kappa_d \rho(x')}{\sqrt{(2R)^2 + (x - x')^2}} dx'. \quad (\text{B3})$$

Because these bound charges are distinguishable from the nanowire charges (cannot tunnel between each other), this potential can be directly transformed into a quantum operator as a Hartree interaction without any Fock correction. Assuming a purely local polarizability (Thomas-Fermi limit), it may be transformed  $\rho(x') \rightarrow \langle \rho(x') \rangle$ , which is perfectly equivalent to the above classical equation. Then, integrating out the bound charges degrees of freedom, the potential is given by:

$$\phi_b(x) = \int \langle \rho(x') \rangle V_b(x, x') dx', \quad (\text{B4})$$

where  $V_b(x, x') \equiv \kappa_d / 4\pi\epsilon\epsilon_0 \sqrt{(2R)^2 + (x - x')^2}$  encodes the geometry information of the interaction.

*Two opposite infinite facets.*— We consider the interface between the nanowire with two opposite infinity facets with different dielectric permittivities  $\epsilon_d$  and  $\epsilon_a$ . Following the previous subsection, the potential  $V_b$  for just one real charge is going to be obtained, and then the results may be generalized to an arbitrary density  $\rho(x)$  and to its corresponding quantum expression. In order to satisfy the boundary condition between the original charge  $q$  and each interface, two image charges  $\kappa_d q$  and  $\kappa_a q$  have to appear in each dielectric medium at the same distance  $R$  from the interface. However, each image charge does not satisfy the boundary condition with the opposite interface. For this reason, two (accidentally equals) additional image charges  $\kappa_d \kappa_a q$  are needed at a distance  $3R$  from each interface (distance between image charge and opposite interface). But these additional image charges neither satisfy the boundary conditions with the opposite interfaces... One can realize that for each image charge  $q_{\alpha,n}$  (in  $q$  charge units) created at the  $n$  step of the image method procedure in the  $\alpha$  dielectric, another image charge,

$$q_{\beta,n+1} = \kappa_\beta q_{\alpha,n}, \quad (\text{B5})$$

with  $q_0 \equiv 1$ ; is created in the opposite  $\beta$  dielectric at a distance  $2nR$  from the original charge  $q$  in order to satisfy the boundary conditions.

*One rectangular corner.*— This problem can be also found in some university student's books[26]: a charge  $q$  is put at a distance  $R_1$  from dielectric  $\epsilon_d$  and at a different distance  $R_2$  from dielectric  $\epsilon_a$ , which is perpendicular to the other one. Two image charges  $\kappa_d q$  and  $\kappa_a q$  have to appear in each dielectric at  $(x, 2R_1, 0)$  and  $(x, 0, 2R_2)$  from the interface. Because of that, another two image charges appear at the same place  $(x, 2R_1, 2R_2)$ . But these two charges are exactly the same: both are  $\kappa_a \kappa_d q$ .

Then, this charge satisfies both boundary conditions at the same time, and therefore there are just three image charges in this system.

*Four rectangular corners: interaction without the leads.*— A charge is placed at the same distance  $R$  from four flat dielectric mediums with dielectric permittivities  $\epsilon_a$ ,  $\epsilon_b$ ,  $\epsilon_c$  and  $\epsilon_d$ . It has been shown that for each image charge, another appear in the opposite interface; while for each two image charges place in two perpendicular interfaces, just one more appears in the corner. Due to this rectangular geometry, image charges appear just at certain points, what gives a potential:

$$V_b(x) = \frac{1}{4\pi\epsilon_0} \left[ \sum_{n,m=1}^{\infty} \left( \frac{(q_{d,n} + q_{a,n})(q_{b,m} + q_{c,m})}{\sqrt{x^2 + (2nR)^2 + (2mR)^2}} \right) + \sum_{n=1}^{\infty} \left( \frac{q_{d,n} + q_{a,n} + q_{b,n} + q_{c,n}}{\sqrt{x^2 + (2nR)^2}} \right) \right], \quad (\text{B6})$$

where:

$$\begin{cases} q_{a,n+1} = \kappa_a q_{d,n} & q_{d,n+1} = \kappa_d q_{a,n} \\ q_{c,m+1} = \kappa_c q_{b,m} & q_{b,m+1} = \kappa_b q_{c,m} \\ q_{\alpha,0} = 1 \leftarrow \forall \alpha = \{a, b, c, d\}. \end{cases} \quad (\text{B7})$$

Because just one charge is needed in the corners in order to satisfy two boundary conditions, number of charges increase in each  $n$  image method step as  $V_b^{(n)} \sim 4n$  (square's perimeter), while potential decreases (for large  $n$ ) as  $V_b^{(n)} \sim \kappa^n/n$ . Then, potential converges.

*General solution: full model interaction.*— Finally, the full system of Fig.(1) is solved. Following the same procedure, the most general bound charges potential is given by:

$$V_b(x) = \frac{1}{4\pi\epsilon_0} \left[ \sum_{n,m,k=0}^{\infty} \left( \frac{q_{k,M_1}(q_{d,n} + q_{a,n} - \delta_{n,0})(q_{b,m} + q_{c,m} - \delta_{m,0})}{\sqrt{(2L - 2^{\text{floor}(\frac{2k+5}{4})}L + (-1)^k x)^2 + (2nR)^2 + (2mR)^2}} + \frac{(q_{k,M_2} - \delta_{k,0})(q_{d,n} + q_{a,n} - \delta_{n,0})(q_{b,m} + q_{c,m} - \delta_{m,0})}{\sqrt{(2^{\text{floor}(\frac{2k+3}{4})}L + (-1)^k x)^2 + (2nR)^2 + (2mR)^2}} \right) \delta_{n+m+k,0} \right], \quad (\text{B8})$$

where:

$$\begin{cases} q_{M_1,n+1} = \kappa_{M_1} q_{M_2,n} & q_{M_2,n+1} = \kappa_{M_2} q_{M_1,n} \\ q_{\alpha,0} = 1 \leftarrow \forall \alpha = \{M_1, M_2\}. \end{cases} \quad (\text{B9})$$

If  $L$  is enough large compare to  $R$  (our case), just lowest order of the new image charges  $q_{M_i}$  terms will contribute

to the potential, so the number of charges increase as  $V_b^{(n)} \sim 12n$ , and then, it still converges. If this is not true ( $L \sim 2R$ ), then the number of charges increase as  $V_b^{(n)} \sim 6n^2$  (cubic's area). Since the potential decreases (for large  $n$ ) as  $V_b^{(n)} \sim \kappa^n/n$ , convergence is not always ensured.

- 
- [1] P.A.M. Dirac, *Proc. R. Soc.* **126**, 360 (1930).
- [2] M. Ettore, *Il Nuovo Cimento* **14** (4), 171 (1937).
- [3] Tena Dubcek, Colin J. Kennedy, Ling Lu, Wolfgang Ketterle, Marin Soljacic and Hrvoje Buljan, *Phys. Rev. Lett.* **114**, 22530 (2015).
- [4] J. Alicea, *Rep. Prog. Phys.* **75**, 076501 (2012).
- [5] R. M. Lutchyn, J. D. Sau, and S. Das Sarma, *Phys. Rev. Lett.* **105**, 077001 (2010).
- [6] V. Mourik, K. Zuo, S. M. Frolov, S. R. Plissard, E. P. A. M. Bakkers, L. P. Kouwenhoven, *Science* **336**, 1003 (2012).
- [7] S. M. Albrecht, A. P. Higginbotham, M. Madsen, F. Kuemmeth, T. S. Jespersen, J. Nygård, P. Krogstrup and C. M. Marcus, *Nature* **531**, 206 (2016).
- [8] H. Zhang et al., e-print arXiv:1603.04069v1 (2016).
- [9] Anindya Das, Yuval Ronen, Yonatan Most, Yuval Oreg, Moty Heiblum, and Hadas Shtrikman, *Nature Physics* **8**, 887 (2012).
- [10] M. T. Deng, C. L. Yu, G. Y. Huang, M. Larsson, P. Caroff, and H. Q. Xu, *Nano Lett.* **12**, 6414 (2012).
- [11] T. D. Stanescu and S. Das Sarma, *Phys. Rev. B* **87**, 180504(R) (2013).
- [12] W. Chang, S. M. Albrecht, T. S. Jespersen, F. Kuemmeth, P. Krogstrup, J. Nygård and C. M. Marcus, *Nature Tech.* **10**, 232 (2015).
- [13] J. Klinovaja and D. Loss, *Phys. Rev. B* **86**, 085408 (2012).
- [14] C. Nayak, S. Simon, A. Stern, M. Freedman, and S. Das Sarma, *Rev. Mod. Phys.* **80**, 1083 (2008).
- [15] S. D. Sarma, M. Freedman, and C. Nayak, *Npj Quantum Information* **1**, 15001 EP (2015).
- [16] F. Domínguez, J. Cayao, P. San-Jose, R. Aguado, A. Levy Yeyati, E. Prada, *npj Quantum Materials* **2**, 13 (2017).
- [17] A. Vuik, D. Eeltink, A. R. Akhmerov, and M. Wimmer, *New J. Phys.* **3**, 033013 (2016).
- [18] M. Tinkham, Introduction to Superconductivity, 2nd ed. (*McGraw-Hill, Inc.* 1996).
- [19] O. Rader and G. Bihlmayer, *New J. Phys.* **17**, 050202 (2015).
- [20] H. A. Nilsson et al., *Nano Lett.* **9**, 3151 (2009).
- [21] M. Hövel, M. Alws, B. Gompf and M. Dressel, *Phys. Rev. B* **81**, 035402 (2010).
- [22] H. J. Suominen, M. Kjaergaard, A. R. Hamilton, J. Shabani, C. J. Palmstrøm, C. M. Marcus, and F. Nichele, e-print arXiv:1703.03699 (2017).
- [23] E. Prada, R. Aguado, P. San-Jose, e-print arXiv:1702.02525 (2017).
- [24] M. T. Deng, S. Vaitiekenas, E. B. Hansen, J. Danon, M. Leijnse, K. Flensberg, J. Nygård, P. Krogstrup, and C. M. Marcus, *Science* **354**, 1557 (2016).
- [25] J. R. Reitz, F. J. Milford and R. W. Chrysty, Foundations of Electromagnetic Theory, 4th ed. (*Addison-Wesley Pub. Co.*, 1967).
- [26] D. J. Griffiths, Introduction to Electrodynamics, 3rd ed. (*Prentice Hall*, 2007).
- [27] In our work, it is considered induced pairing amplitude does not change with the magnetic field. However, it has been taking into account by: T. D. Stanescu and S. Das Sarma, e-print arXiv:1702.03976 (2017).
- [28] Differential conductance is usually showed in units of  $2e^2/h$ , which is the conductance through the wire between a normal lead and a SC one at vanishing bias voltage and temperature.